Revisiting the He II to H I ratio in the intergalactic medium

S. Muzahid, R. Srianand, P. Petitjean

HAL Id: insu-03646061
https://insu.hal.science/insu-03646061

Submitted on 21 Apr 2022

Revisiting the He II to H I ratio in the intergalactic medium

S. Muzahid,[1]★ R. Srianand[1] and P. Petitjean[2]

[1]*Inter-University Centre for Astronomy and Astrophysics, Post Bag 4, Ganeshkhind, Pune 411 007, India*
[2]*Université Paris 6, UMR 7095, Institut d'Astrophysique de Paris-CNRS, 98bis Boulevard Arago, 75014 Paris, France*

ABSTRACT

We estimate the He II to H I column density ratio, $\eta = N(\text{He\,II})/N(\text{He\,I})$, in the intergalactic medium towards the high-redshift ($z_{\text{em}} = 2.885$) bright quasar QSO HE 2347−4342 using Voigt-profile fitting of the H I transitions in the Lyman series and the He II Lyman α transition as observed by the *FUSE* satellite. In agreement with previous studies, we find that $\eta > 50$ in most of the Lyman α forest, except in four regions where it is much smaller ($\eta \sim 10$–20) and therefore inconsistent with photoionization by the ultraviolet background flux. We detect O VI and C IV absorption lines associated with two of these regions ($z_{\text{abs}} = 2.6346$ and 2.6498).

We show that, if we constrain the fit of the H I and/or He II absorption profiles with the presence of metal components, we can accommodate η values in the range 15–100 in these systems, assuming that broadening is intermediate between pure thermal and pure turbulent.

While simple photoionization models reproduce the observed $N(\text{O\,VI})/N(\text{C\,IV})$ ratio, they fail to produce low η values, in contrast to models with high temperatures (i.e $T \geq 10^5$ K). The Doppler parameters measured for different species suggest a multiphase nature of the absorbing regions. Therefore, if low η values were to be confirmed, we would favour a multiphase model in which most of the gas is at a high temperature ($>10^5$ K) but the metals, and in particular C IV, are due to a lower-temperature ($\sim$few 10^4 K) photoionized gas.

Key words: intergalactic medium – quasars: absorption lines – quasars: individual: HE 2347−4342.

1 INTRODUCTION

The presence of metals in the H I Lyman α forest at optical depths $\tau_{\text{Ly}\alpha} \geq 1$, detected through C IV and O VI absorption lines seen in quasi-stellar object (QSO) spectra, is now well established (see Songaila & Cowie 1996; Bergeron et al. 2002; Simcoe, Sargent & Rauch 2004).

Observations are consistent with an average carbon metallicity relative to solar of [C/H] ~ -2.8, with no sign of redshift evolution over the range $1.8 \leq z \leq 4.1$, but a significant trend with overdensities (Schaye et al. 2003; Aguirre et al. 2008).

Given the expected low metallicities and the high ionization state of the gas, direct detection of metal absorption lines from underdense regions of the intergalactic medium (IGM) is beyond the scope of present-day large telescopes. Statistical methods such as pixel analysis are used instead (Ellison et al. 2000; Schaye et al. 2003; Aracil et al. 2004; Scannapieco et al. 2006; Pieri et al. 2010) and show that metals must be present in the low-density regions. Even in regions where C IV absorption is detected directly, it is not clear what main physical process is maintaining the ionization state of the gas. In general, it is believed that photoionization keeps

the gas ionized. However, it is probable that mechanical inputs from galactic winds can influence the ionization state of part of the IGM gas through collisional ionization, at least in the proximity of galaxies. Therefore, it is important to study simultaneously different species covering a wide range of ionization states to obtain a better understanding of the metal enrichment and the various ionizing mechanisms at play.

Recent hydrodynamical simulations (Davé et al. 2001; Fang & Bryan 2001; Kang et al. 2005; Bouché, Lehnert & Péroux 2006; Bouché et al. 2007) suggest that the missing baryons at low redshift, $z \sim 0$–0.5, and the missing metals at high redshift, $z \sim 2.5$, could reside in the warm–hot phase of the intergalactic medium (the so-called WHIM, with $T \approx 10^5$–10^7 K). Highly ionized species of oxygen such as O VI, O VII and O VIII can be useful probes of the WHIM. While the strongest transitions of the latter two species have rest wavelengths in the soft X-ray range, the spectral doublet O VI $\lambda\lambda$1032, 1037 is seen in the near-ultraviolet (UV) range and is therefore a useful probe of gas at a temperature of $\sim 3 \times 10^5$ K, the temperature at which O^{5+}/O is maximum.

It has been suggested that a large fraction of the conspicuous O VI phase seen to be associated with high-redshift damped Lyman α (DLA) systems may originate from collisionally ionized gas (Fox et al. 2007). However, photoionization can also maintain oxygen in a high ionization state and at relatively low temperatures ($T \sim$ a few

★E-mail: sowgat@iucaa.ernet.in

10^4 K; see Oppenheimer & Davé 2009). Actually, a large fraction of the O VI absorption seen at $z > 2.5$ in quasars shows Doppler broadening consistent with photoionization in the vicinity of the QSOs (e.g. Srianand & Petitjean 2000) but also in the diffuse IGM (e.g. Bergeron et al. 2002; Simcoe et al. 2004). While it is expected that the intrinsic ionizing spectra of QSOs will be hard enough to maintain a high degree of ionization of oxygen in their vicinity, in the IGM the hardness of the ionizing spectrum will depend on the intrinsic spectral shape of the ionizing sources and the IGM opacity at the H I and He II Lyman limit (Haardt & Madau 1996; Fardal, Giroux & Shull 1998).

An additional piece of information comes from QSO lines of sight transparent in the Lyman continuum [i.e high-z QSO lines of sight without any intervening Lyman limit system (LLS) blocking the UV end of the spectrum]. It is then possible to observe the rest-wavelength ranges of the H I and He II Lyman α forests and to compute the ratio of the He II to the He I optical depth (i.e the η parameter). The bright QSO HE 2347−4342 at $z_{em} = 2.885$ (Reimers et al. 1997) is one such target that has attracted much attention in recent years. It has been shown that the He II opacity is 'patchy' in nature (Reimers et al. 1997; Smette et al. 2002) and that η decreases gradually from higher to lower redshifts, possibly owing to a change in the slope of the ionizing spectrum (Zheng et al. 2004). Shull et al. (2004) discussed the small-scale variations (over $\Delta z \approx 10^{-3}$) of η and found an apparent correlation between high η (less ionized He II) and low He I column density. They ascribed these small-scale η variations to 'local ionization effects' in the proximity of QSOs located close to the line of sight and having spectral indices ranging from $\alpha_s = 0$ to 3. Worseck et al. (2007) reported the detection of 14 foreground QSOs in the field located close to the line of sight and could not find any convincing evidence for any transverse proximity effect from a decrease in the He I absorption, although they did claim that the local UV spectrum inferred in the vicinity of three foreground QSOs appeared harder than expected, which is an indication of a transverse proximity effect. In turn, these fluctuations could result from an appreciable contribution of thermal broadening to the velocity width of absorption lines at high N(H I) (Fechner & Reimers 2007).

In this paper, after a description of the observations (Section 2), we use a different approach involving Voigt-profile-fitting analysis of the H I and He II absorption lines to measure η (Section 3). We then report new detections of O VI absorption associated with regions with low η values (Section 4) and construct models of these regions (Section 5), before concluding in Section 6.

2 OBSERVATIONS

The optical spectrum of HE 2347−4342 ($z_{em} = 2.885$) used in this study was obtained with the VLT UV Echelle Spectrograph (UVES) (Dekker et al. 2000) mounted on the ESO Kueyen 8.2-m telescope at Paranal Observatory in the course of the ESO–VLT large programme 'The Cosmic Evolution of the IGM' (Bergeron et al. 2004). HE 2347−4342 was observed through a 1-arcsec slit (with a typical seeing of 0.8 arcsec) for 12 h with central wavelengths adjusted to 3460 and 5800 Å in the blue and red arms, respectively, using dichroic no. 1, and for another 14 h with central wavelengths at 4370 and 8600Å in the blue and red arms with dichroic no. 2. The raw data were reduced using the latest version of the UVES pipeline (Ballester et al. 2000), which is available as a dedicated context of the MIDAS data-reduction software. The main function of the pipeline is to perform a precise inter-order background subtraction for science frames and master flat-fields, and to apply an

optimal extraction to retrieve the object signal, rejecting cosmic-ray impacts and performing sky subtraction at the same time. The reduction is checked step-by-step. Wavelengths are corrected with vacuum-heliocentric values, and individual one-dimensional spectra are combined. Air-vacuum conversions and heliocentric corrections were performed using standard conversion equations (Edlén 1966; Stumpff 1980). The addition of individual exposures was performed by adjusting the flux in individual exposures to the same level and inverse-variance-weighting the signal in each pixel. Great care was taken in computing the error spectrum when combining the individual exposures. Our final error in each pixel is the quadratic sum of the weighted mean of errors in the different spectra and the scatter in the individual flux measurements. Errors in individual pixels obtained by this method are consistent with the rms dispersion around the best-fitting continuum in regions free of absorption lines. The final combined spectrum covers the wavelength range 3000 to 10 000 Å. A typical signal-to-noise ratio ∼60 per pixel (of 0.035 Å) is achieved over the whole wavelength range of interest for a spectral resolution of $R \sim 45\,000$. A detailed quantitative description of the data calibration is presented in Aracil et al. (2004) and Chand et al. (2004).

We use the continuum-normalized *FUSE* data provided by Dr W. Zheng. The details of the data reduction and continuum normalization can be found in Zheng et al. (2004).[1] The original data have a typical resolution of $R = 20\,000$ and a signal-to-noise ratio ∼5 in the long-wavelength range ($\lambda > 1050$ Å). Following Zheng et al. (2004), we re-binned these data to 0.1 Å, which leads to an effective resolution of $R \sim 4000$. We restrict ourselves to the wavelength range with a signal-to-noise ratio >10. This corresponds to a redshift range $2.58 \leq z \leq 2.70$, or a velocity range of ∼10 000 km s^{-1} around a central redshift of $z = 2.6346$ (see Fig. 1).

3 N(He II)/N(He I) RATIO

In this section we concentrate on the column density ratio $\eta = N$(He II)/N(H I) over the redshift range $2.58 \leq z \leq 2.70$, where the *FUSE* data show a relatively good signal-to-noise ratio. This range roughly corresponds to a relative velocity range of -4000 to $+5000$ km s^{-1} around the strong O VI absorber seen at $z_{abs} = 2.6346$ (see Fig. 1).

As a first step, we simultaneously fitted the Lyman α to Lyman γ profiles when possible, for example when the Lyman β and/or Lyman γ lines are not blended with another intervening Lyman α line. Then we compared the He II absorption profile with a model with the same components as the H I model, scaling the fitted H I column densities by the parameter η. We considered two alternatives: in the first case we used the same Doppler parameter for H I and He II (assuming turbulent broadening); in the second case we

---

[1] We obtained individual spectra reduced using CALFUSE 3.2.1 from http://fuse.iap.fr/interface.php. We combined lithium fluoride (LIF) spectra after correcting for the background by demanding zero flux in the core of strong saturated absorptions in the wavelength range 1130–1185 Å. When we follow the same continuum fitting and re-binning procedures as Zheng et al. (2004), we find that the new data follow the structures (both in wavelength and in flux) seen in the data of Zheng et al. (2004) very well and that the fitting results are not changed. Thus, the results presented in this paper will not change when the new pipeline is used for the data reduction. After this work was completed, new Cosmic Origins Spectrograph (COS) data on this object were reported by Shull et al. (2010). As the *COS* spectrum is found to be consistent (see their fig. 3) with the *FUSE* spectra used here, this has no consequences for the results of this paper.
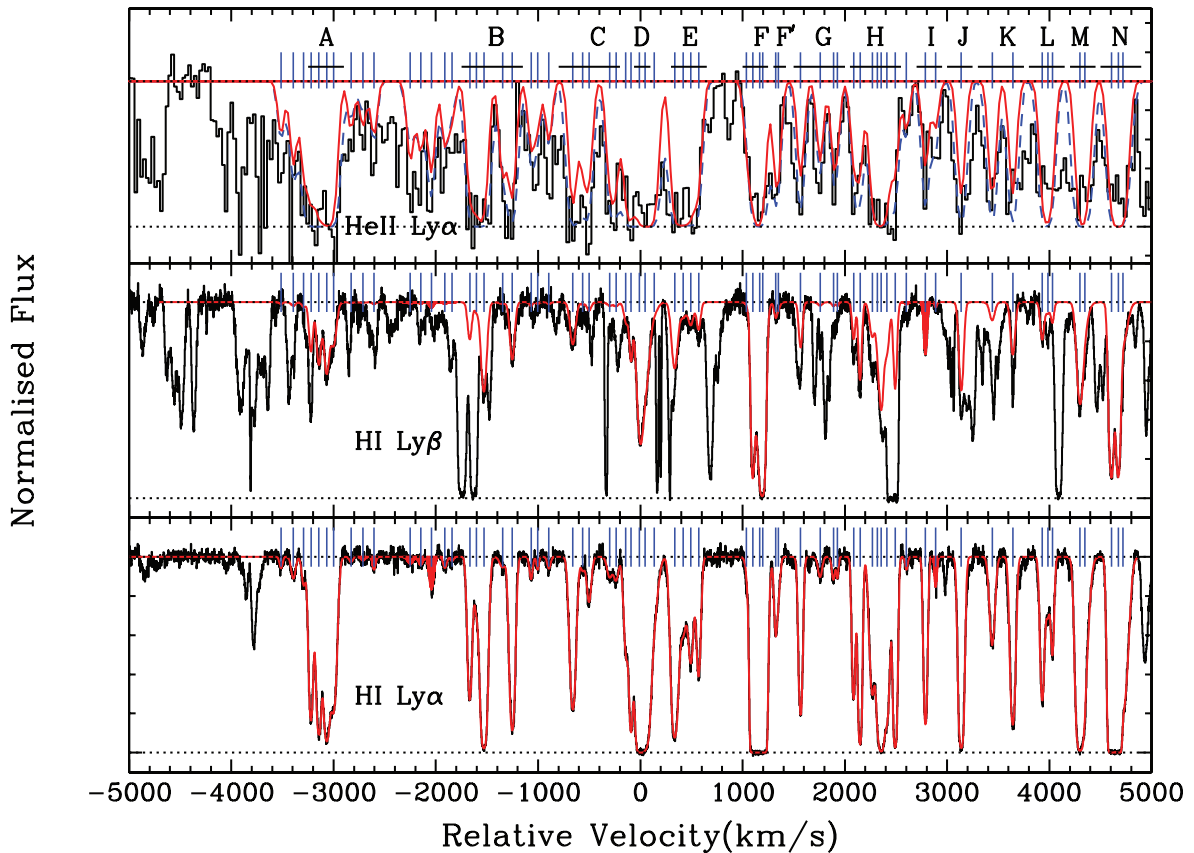
Figure 1. H I and He II Lyman α and H I Lyman β absorption profiles on a velocity scale with origin $z = 2.6346$. Various velocity ranges in which η is measured through χ^2 minimization are indicated with horizontal lines and labelled by letters in alphabetical order from left to right. Vertical tick marks located above the absorption profiles show the positions of the individual Voigt-profile components used to fit the Lyman α and Lyman β H I lines together. The best-fitting models for H I Lyman β and Lyman α are overplotted on the data. The *FUSE* spectrum is shown in the top panel, together with the best-fitting profile obtained from scaling the H I column densities by the fitted η parameter and assuming thermal (solid red line) or turbulent (dashed blue line) broadening for the He II lines.

gave the He II b-parameter the value expected from thermal broadening [i.e $b(\text{He II}) = 0.5\, b(\text{H I})$]. The best-fitting values of η were obtained by χ^2-minimization. While fitting the He II profiles we used a Gaussian convolving function to correctly represent the *FUSE* spectral resolution. For Voigt-profile decomposition we used the fitting code developed by Khare et al. (1997).

As the *FUSE* data are of much lower resolution and signal-to-noise ratio than the UVES data, we cannot estimate η for individual H I components. Instead, we singled out 15 small regions, termed A, B, C etc. in Fig. 1, and derived the best η value over each region. We note that the approach we have taken here is very different from that in previous studies. Indeed, Shull et al. (2004) used the apparent optical depth (AOD) method in Lyman α only, whereas Kriss et al. (2001) and Zheng et al. (2004) used Gaussian decomposition, and Fechner & Reimers (2007) scaled the whole He I spectrum by $\eta = 4\tau_{\text{He II}}/\tau_{\text{H I}}$ to fit the He II data. In all these studies, only H I Lyman α is used.[2] The simultaneous fitting of the H I optical depths in all available Lyman series lines allows us to discriminate between thermal and turbulent broadening.

The best-fitting Voigt profiles to the Lyman α and Lyman β absorption lines are shown in the bottom and middle panels of Fig. 1.

The top panel shows the best-fitting He II Lyman α line with the two assumptions on the Doppler parameter discussed above. The χ^2 curves as a function of η for the various regions singled out in Fig. 1 are shown in Fig. 2. The solid and dashed lines in these plots represent the cases of thermal and turbulent broadening, respectively. In most cases, the χ^2 curve shows a clear minimum, thereby allowing us to discriminate between the turbulent and thermal cases, and to derive the best-fitting value of η. Errors are estimated from the range of η values corresponding to $\Delta\chi^2 = \pm 1$ around the minimum. There are regions, especially when the He II Lyman α line is saturated, for which the χ^2 curve flattens (e.g. regions E and G), and we have only a one-sided limit. In these cases we define the 2σ lower limit of η as the value corresponding to a χ^2 equal to the χ^2 of the flat part of the curve plus four. The shapes of the χ^2 curves are not symmetric, which is a natural consequence of line saturation.

It is clear from the Fig. 2 that, apart from region I, the χ^2 values are smaller in the case of turbulent broadening and that minima are reached only in that case. In the case of thermal broadening, the χ^2 curves seem to saturate to some asymptotic value, probably because the observed He II profiles are too broad to be reproduced by the model. Thus the exercise presented here shows that the widths of He II Lyman α lines are consistent with the b-parameter derived from H I lines.

If the gas is optically thin and photoionized by a UV background dominated by QSOs, we would expect η to be in the range

---

[2] A limited amount of analysis of Lyman β has been undertaken by Zheng et al. (2004).

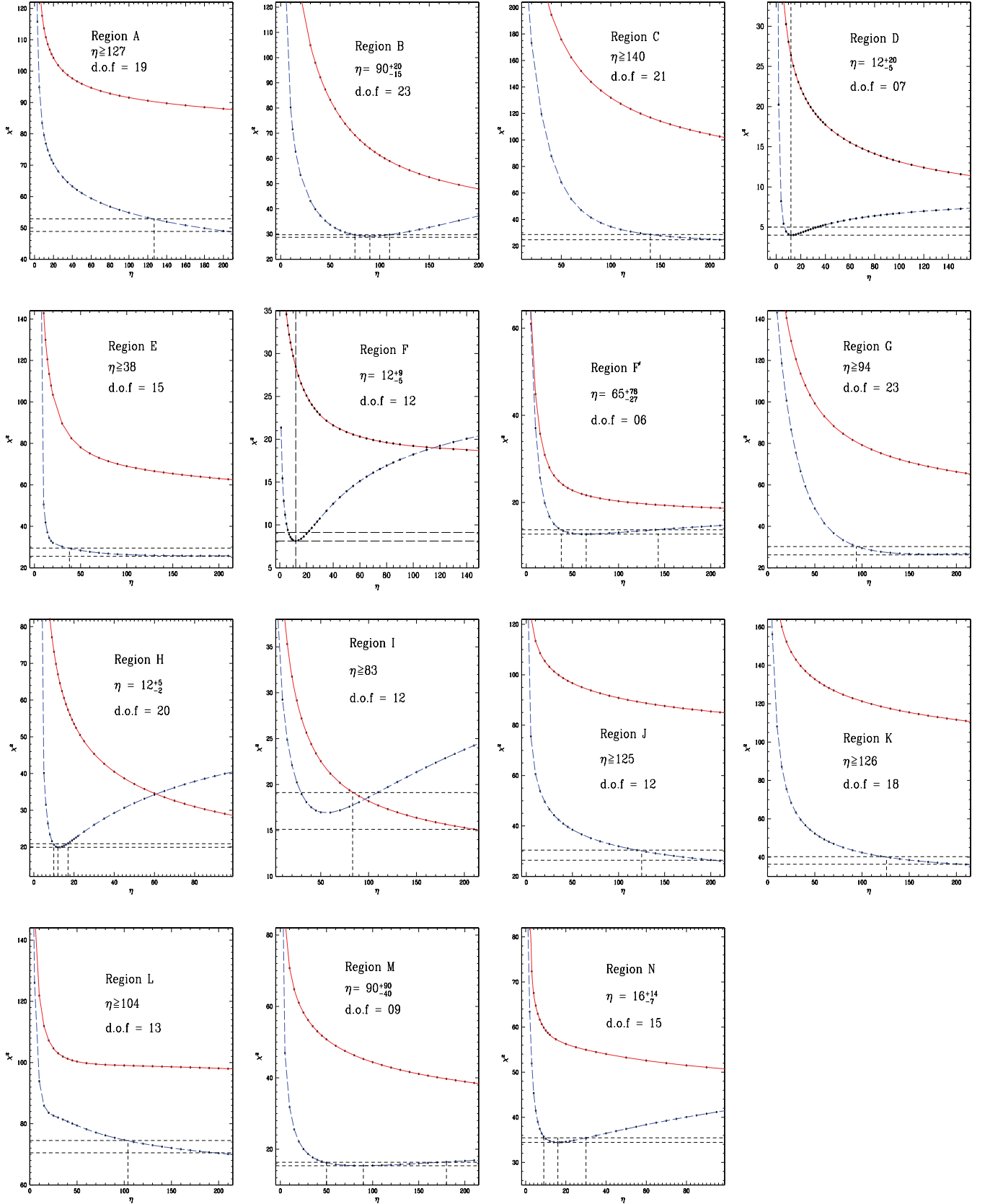**Figure 2.** χ^2 resulting from the comparison of the He II absorption with a model profile obtained by scaling the H I column density with the parameter η as a function of η for the regions defined in Fig. 1. The dashed blue and solid red curves are for the two extreme cases, respectively: $b(\mathrm{He\,II}) = b(\mathrm{H\,I})$ (i.e turbulent broadening) or $b(\mathrm{He\,II}) = 0.5\,b(\mathrm{H\,I})$ (i.e pure thermal broadening).

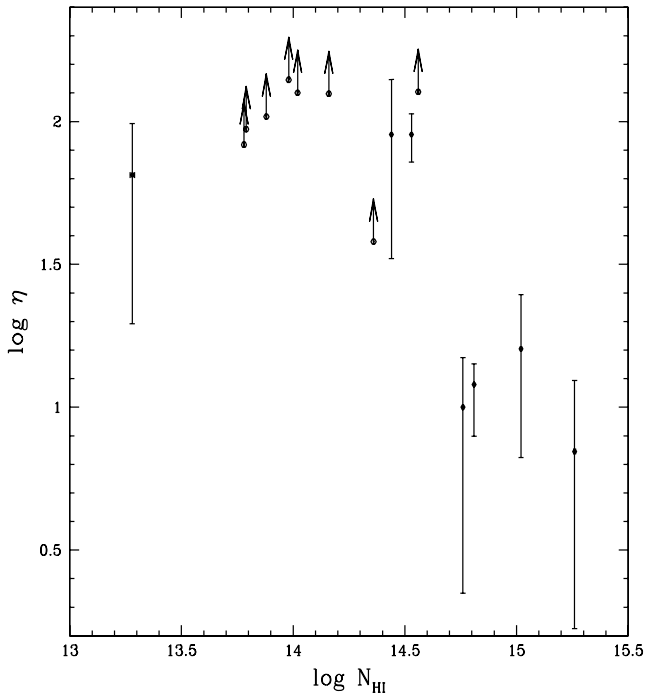**Figure 3.** The η values for the 15 regions delineated in Fig. 1 are plotted against the neutral hydrogen column density.

40–400, depending on the exact spectral index and the IGM opacity. In the case of a self-shielded optically thick gas, η could be even higher (Fardal et al. 1998). Four regions (D, F, H and N) in Fig. 2 have $\eta \leq 40$. These regions are associated with large H I column densities, as can be seen in Fig. 3, where $\log \eta$ is plotted against $\log N(\text{H I})$ as measured in the various regions. This correlation was noted in earlier works. Fechner & Reimers (2007) argued that it can be explained if the thermal broadening of lines is also important.

In the following, we will use additional information on metal lines observed in the UVES spectrum to discuss further the ionization state of the gas in these regions.

4 REGIONS WITH LOW η VALUES

In the previous section, we showed that the $N(\text{He II})/N(\text{H I})$ ratio can be explained over most of the observed spectrum by ionization of the gas by the UV background, except in four regions: D ($z_{abs} = 2.6346$), F ($z_{abs} = 2.6498$), H ($z_{abs} = 2.6624$) and N ($z_{abs} = 2.6910$). The presence of O VI and C IV absorption in systems showing low values of η may yield interesting clues about (i) the nature of the ionizing radiation, (ii) the effect of thermal/turbulent broadening and (iii) the possible mechanical feedback from winds.

Regions D and F are associated with C IV and strong O VI absorption lines. These are the only two C IV systems in the redshift range $2.58 \leq z \leq 2.70$ (see top panels in Fig. 4) and we discuss them in detail below.

For region H, the wavelength range where possible O VI $\lambda 1031$ absorption is redshifted is strongly blended, and only a possible weak line is present at the expected location of O VI $\lambda 1037$ (see Fig. 4c). As no other metal line is detected at this redshift we are unable to confirm if this feature does indeed result from O VI absorption.

For region N, while both O VI regions are strongly blended, the optical depth constraints are satisfied at two velocity positions (see

Fig. 4). However, the possible O VI $\lambda 1031$ feature is also consistent with there being C III absorption at $z_{abs} \sim 2.8972$. Similarly, the possible O VI $\lambda 1037$ line is blended with Lyman β at $z_{abs} = 2.7306$ and O VI $\lambda 1031$ at $z_{abs} = 2.7121$. Hence, we cannot confirm the presence of O VI absorption in this region. Note that in region N (i.e. $z_{abs} = 2.6910$), η is probably affected by a transverse proximity effect from QSO J23495 − 4338 located at redshift $z = 2.690 \pm 0.006$, 15 arcmin from the line of sight of interest (Worseck et al. 2007).

Note that we detect O VI absorption at $z_{abs} = 2.7121$, 2.7356 and 2.7456 as well. The He II opacity is high at $z_{abs} = 2.7121$ and 2.7456, which makes η difficult to estimate. If we scale the Voigt-profile fits to the He I absorption to reproduce the He II profile, we find η to be in the range 10–100 and >100 for, respectively, the systems at $z_{abs} = 2.7121$ and 2.7456. The wavelength range in which the He II absorption at $z_{abs} = 2.7356$ is expected to be redshifted has been removed in Zheng et al. (2004) because of the strong airglow lines, so we cannot estimate η for this system. The system at $z_{abs} = 2.7356$ is a known Lyman-limit system. A Voigt-profile fit to the He I absorption gives $\log N(\text{He I}) = 16.50 \pm 0.28$.

4.1 System at $z_{abs} = 2.6498$

A velocity plot of high-ionization metal lines and H I lines from this system is shown in Fig. 4(b). Clearly, the metal lines are off-centre with respect to the He I absorption. In addition, there is a velocity offset of 2 to 10 km s^{-1} between the centroids of the O VI and C IV absorption profiles. Interestingly, all the shifts are in the same direction as would be expected in a flow ionized from the same side. The best fit of the profiles is obtained when we allow for C IV component redshifts to be independent of those of the O VI components (see Table 1).

Doppler parameters are larger for O VI than for C IV, which supports neither pure thermal nor pure turbulent broadening. The upper limits on the kinetic temperature of the gas measured from the b-parameters of O VI components are 1.4×10^6, 8×10^4, 1.2×10^5 and 4×10^4 K, respectively, for components at -76.2, -48.6, -20.2 and $+4.2$ km s^{-1}. Therefore, within the allowed error in b-parameters, the O VI profile allows for the existence of high temperatures ($T > 10^5$ K), at least in part of the associated gas.

Fig. 5(a) shows the apparent column densities of O VI (in blue) and C IV (in red) per unit velocity interval versus relative velocity. Because O VI $\lambda 1037$ is heavily blended we used only the O VI $\lambda 1031$ line.

For C IV, we used the oscillator-strength weighted mean of the column densities per unit velocity measured from both absorption lines of the doublet. For clarity, we multiplied the C IV apparent column density profile by a factor of 10. Vertical dashed and dotted lines show the positions of peaks in the optical depth of C IV and O VI, respectively. It is apparent that the O VI peaks are shifted compared with the C IV ones.

In Fig. 5(b) we plot the ratio of O VI to C IV apparent column densities per unit velocity against the relative velocity and find that the ratio varies between 10 and 20 through the C IV absorption profile. The fact that the O VI absorption profile is broader suggests the existence of gas outside the C IV profile with the O VI to C IV column density ratio higher than 20.

The component at $\sim +4.2$ km s^{-1} has virtually no detectable H I absorption associated with it. From the Lyman α line we derive an upper limit of $\log N(\text{H I}) = 12.80$, suggesting that metallicity is probably high in this component. Indeed, given the low b value of the component, it is probable that the gas is photoionized, in which
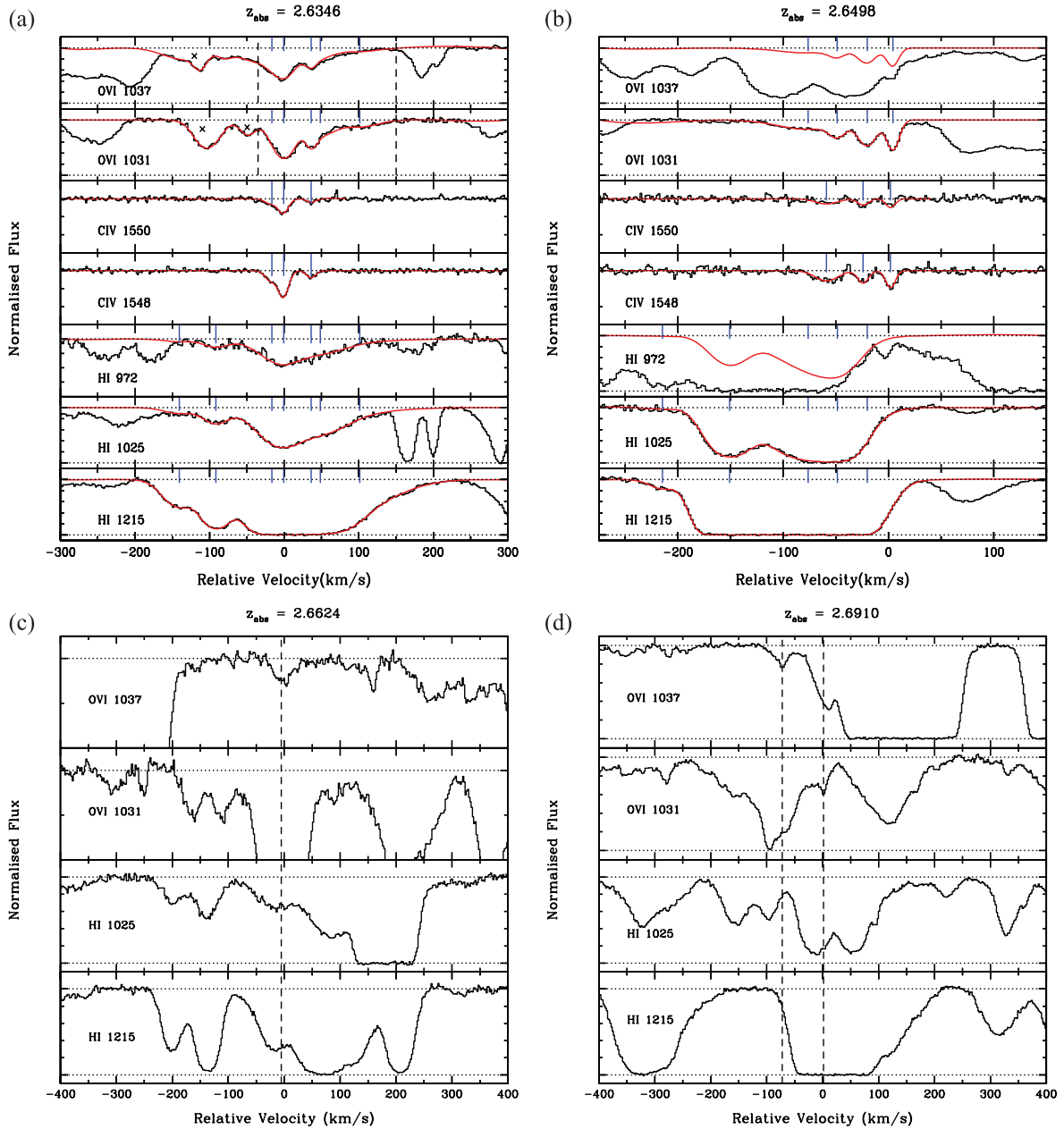
Figure 4. Absorption profiles are shown on a velocity scale for regions with low η values (see Fig. 1): D, F (upper left- and right-hand-side panels) and H, N (lower left- and right-hand-side panels). C IV and O VI are clearly detected in regions D and F. In these cases we also overplot the best-fitting Voigt-profile model and indicate individual components with vertical tick marks. For regions H and N, there are only tentative O VI coincidences. Vertical dashed lines in the bottom panels mark the locations of tentative O VI doublet components. The vertical dashed lines in (a) delineate the region of O VI absorption. Regions marked by '×' are Lyman α contamination.

case the metallicity has to be close to solar. For the other three components that coincide with a strong H I absorption it is impossible to quantify the amount of H I absorption associated with them individually such that useful metallicity limits can be established.

We have seen above (Fig. 2) that the χ^2 curve corresponding to the fit of the He II absorption shows a marked minimum for $\eta = 12$ in the case of turbulent broadening (i.e $\xi = b_{\text{He II}}/b_{\text{He I}} = 1$) and no minimum for pure thermal broadening ($\xi = 0.5$). In Fig. 6(a) we show the simulated He II profiles for $\eta \sim 130$ and $\xi = 0.5$ (solid curve) and $\eta \sim 12$ and $\xi = 1.0$ (dashed curve). Remember that for these fits we used the minimum number of Voigt-profile components without any constraint from the O VI profile.

It is apparent that the red solid He II profile (obtained assuming pure thermal broadening) is missing several pixels in the red wing of the region of interest around 0 km s^{-1}. This is because the b value of the corresponding component (fixed by the H I profile) must be much larger to reach this position. If we now add the constraint that H I should be associated with the three O VI components, we can reproduce this profile better. Indeed, because of the extra component at $v \sim -20$ km s^{-1}, the pure thermal-broadened He II profile with higher η (~ 100) gives an equally good fit (Fig. 6c).

It seems, therefore, that if we add a He II component at the position of the redder O VI component, any value of η between ~ 15 and 100 is acceptable. Thus it seems that the possible presence of

Table 1. Results of multiple-component Voigt-profile fitting to the $z_{abs} = 2.6498$ system. The parameters for H I are obtained by keeping the component structure as seen in O VI.

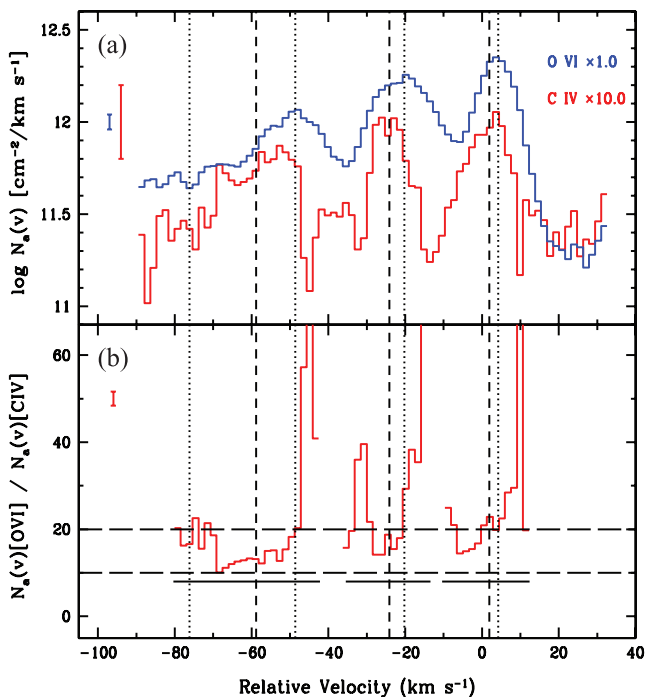| v (km s^{-1})	Ion	H I lines used	b (km s^{-1})	$\log N$ (in cm^{-2})
-214.6 ± 1.0	H I	Lyα	16.3 ± 1.5	12.59 ± 0.03
-150.8 ± 0.3	H I	Lyα, Lyβ	23.6 ± 0.3	14.63 ± 0.01
-76.2 ± 0.0	H I	Lyα, Lyβ	37.6 ± 0.9	14.91 ± 0.01
-48.6 ± 0.0	H I	Lyα, Lyβ	23.1 ± 0.7	14.68 ± 0.02
-20.2 ± 0.0	H I	Lyα, Lyβ	26.4 ± 1.1	13.53 ± 0.06
-76.2 ± 3.3	O VI		38.6 ± 3.9	13.56 ± 0.05
-58.8 ± 1.0	C IV		14.5 ± 1.5	12.30 ± 0.03
-48.6 ± 0.3	O VI		9.4 ± 0.9	13.16 ± 0.06
-24.1 ± 0.6	C IV		5.9 ± 1.0	12.06 ± 0.04
-20.2 ± 0.2	O VI		10.9 ± 0.4	13.55 ± 0.02
$+1.9 \pm 0.4$	C IV		4.8 ± 0.7	12.16 ± 0.03
$+4.2 \pm 0.1$	O VI		6.5 ± 0.2	13.49 ± 0.01

Figure 5. (a) Apparent column density profiles of O VI (in blue) and C IV (in red) per unit velocity interval versus relative velocity for the system $z_{abs} = 2.6498$. For display purposes, C IV apparent column densities have been multiplied by a factor of 10. The mean errors in each pixel for O VI (blue error bar) and C IV (red error bar) are shown on the left. (b) Apparent column density ratio through the profile. The error bar on the left shows the corresponding mean error in each pixel. Vertical dotted lines show the centroids of Voigt components. The shift between the O VI and C IV centroids is apparent.

unresolved narrow H I components could be one of the causes of low η measurements. It is a fact, however, that the main H I components have large b values, corresponding to temperatures in excess of 10^5 K. Therefore it is not impossible that part of the gas is at a high temperature.

4.2 System at $z_{abs} = 2.6346$

Absorption profiles from this system are shown on a velocity scale in Fig. 4. Unlike in the previous system, the velocity range of metal lines falls well within the Lyman α profile.

The O VI $\lambda1037$ line is blended with Lyman γ at $z = 2.8781$ and with Lyman β at $z = 2.6765$. Because of this contamination, we use the well-measured redshifts of C IV components to fit the O VI doublet. The contributions of the contaminating lines are self-consistently computed using other available transitions. In addition to the C IV counterparts, we need two components in the red part of the profile to fit the O VI doublet where there is no C IV absorption. H I Lyman α, Lyman β and Lyman γ lines have been fitted simultaneously, imposing components at the redshifts of five O VI components. Two extra components are required in the blue (~ -100 km s^{-1}) to cover the total He I absorption. The details of the fit results are given in Table 2.

As in the previous system, for the components with both C IV and O VI, the O VI b-parameters are larger than the C IV ones, and the column density ratio of O VI to C IV is as high as ~15. The O VI b-parameters correspond to upper limits on the kinetic temperature of 4×10^5, 3×10^5 and 9×10^4 K, respectively, for the components at -16.4, -0.6 and $+36.2$ km s^{-1}. In the components where we find only O VI, the ratio of O VI to C IV column densities can be higher than 20. These components have broad O VI lines with b-parameters corresponding to upper limits of 6×10^5 and 10^6 K, respectively, for components at $+48$ and $+101$ km s^{-1}. The corresponding H I components also have high b values, allowing for high temperatures ($\sim10^5$ K) in the gas associated with these two components. All this suggests a multiphase structure in this absorbing gas, with the possible existence of a hot phase contributing to most of the O VI absorption. Indeed, the O VI profile is suggestively broad.

We fitted the H I and He II profiles in the two extreme cases of pure turbulent and pure thermal broadening, considering both components from the fit of the H I profile only and from the fit of metal lines. The results are given in Fig. 7 and Table 2. We note from Fig. 7(c) that, even when we tie the H I components to O VI components, the best-fitting χ^2 is obtained for the pure turbulent case with low η. However, reality probably corresponds to an intermediate case with ξ between 0.5 and 1. In Fig. 8(b) we plot the minimum χ^2 value obtained for various values of ξ. Even though the best-fitting χ^2 value is obtained for $\xi = 1$, the curve is flat and the 1σ range is $\xi \geq 0.6$. As can be seen in the top panel of the figure, this can accommodate a wide range of η. Therefore, in this system also high η values are acceptable, although H I and O VI absorption profiles are broad and highly suggestive of a gas with temperature higher than the typical photoionization temperature (i.e a few 10^4 K).

5 MODELS

Given the particularities of the systems singled out by the presence of O VI absorption, namely possible low η values and high O VI/C IV ratios, we constructed models to test the various mechanisms that could induce such properties. It is well known that photoionization by a power-law spectrum with appropriate slope can yield low η values. This would require the presence of local sources of hard photons (see Shull et al. 2004). Observations by Worseck et al. (2007) seem to show, however, that there is no QSO present in the vicinity of the two absorbers considered in the previous section. While this observation does not rule out a QSO emission highly beamed
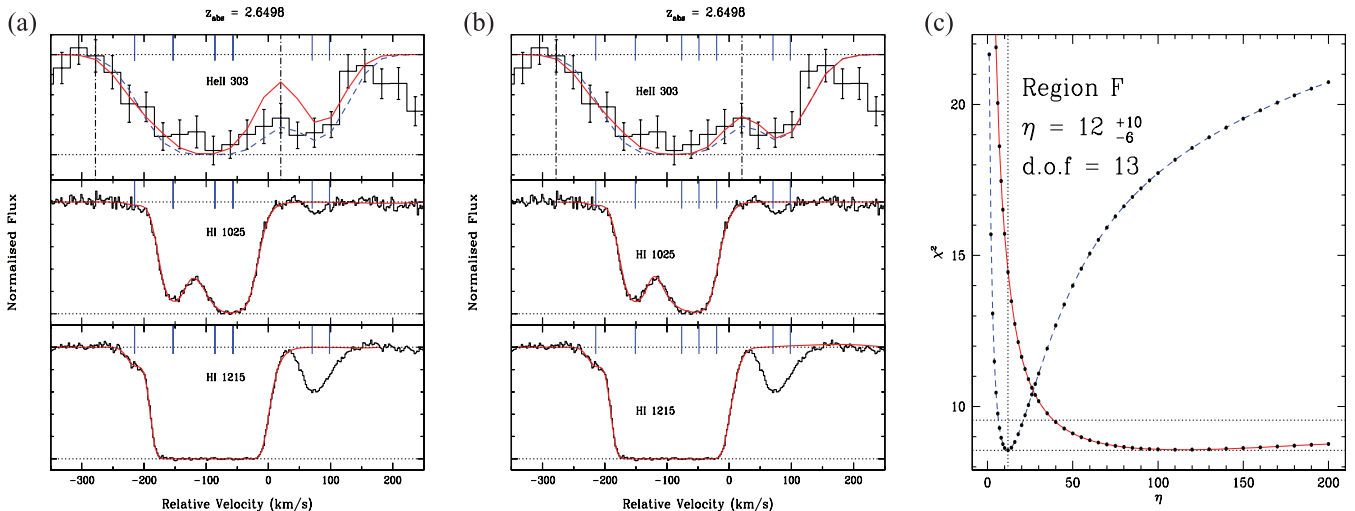
Figure 6. Fits of H I and He II absorption in the $z_{abs} = 2.6498$ system. In all panels, dashed (blue) and solid (red) curves are for turbulent, $\xi = b(\text{He II})/b(\text{H I}) = 1$, and thermal, $\xi = 0.5$, broadening cases respectively. (a) Fit using the minimum number (four) of components required to fit the H I absorption. The dashed and solid curves in the top panel are the simulated He II profiles with $\eta \sim 12$ and 130, respectively. Only pixels between the two vertical dot–dashed lines are used to derive η by χ^2 minimization. (b) Fit with five components imposing H I components at the position of the O VI components. The dashed and solid curves in the top panel are the simulated He II profiles with $\eta \sim 12$ and 100, respectively. Note that two components around $+90$ km s^{-1} are fitted together to take into account their contribution to the He II absorption. For these two components we take $\eta = 65$ and pure turbulent broadening derived from the analysis of region F$'$ (see Fig. 2). (c) χ^2 plot for fits shown in the middle row (b). Vertical ticks in (a) and (b) indicate the positions of individual Voigt components.

Table 2. Component details of the system at $z_{abs} = 2.6346$.

v_0 (km s^{-1})	Ion	H I lines used	b (km s^{-1})	$\log N$ (in cm^{-2})
-140.6 ± 0.0	H I	Lyα	27.8 ± 0.6	13.41 ± 0.01
-91.6 ± 0.0	H I	Lyα ,Lyβ ,Lyγ	22.5 ± 0.3	13.80 ± 0.01
-16.4 ± 0.2	H I	Lyα ,Lyβ ,Lyγ	38.2 ± 0.9	14.27 ± 0.03
	O VI		20.3 ± 8.3	12.76 ± 0.28
	C IV		11.5 ± 2.4	12.55 ± 0.12
-0.6 ± 0.7	H I	Lyα ,Lyβ ,Lyγ	28.3 ± 2.2	14.14 ± 0.06
	O VI		18.9 ± 0.5	14.05 ± 0.02
	C IV		8.1 ± 0.6	12.83 ± 0.06
$+36.2 \pm 0.7$	H I	Lyα ,Lyβ ,Lyγ	25.7 ± 10.4	13.24 ± 0.37
	O VI		9.6 ± 0.8	13.37 ± 0.04
	C IV		7.5 ± 1.0	12.19 ± 0.04
$+48.5 \pm 0.0$	H I	Lyα ,Lyβ ,Lyγ	46.6 ± 1.5	14.32 ± 0.01
	O VI		25.2 ± 1.6	13.61 ± 0.03
$+101.4 \pm 0.0$	H I	Lyα ,Lyβ	69.5 ± 2.0	13.69 ± 0.02
	O VI		32.8 ± 3.5	13.35 ± 0.04

perpendicular to the line of sight or a short-lived QSO emission in the vicinity of the absorbers, we explore alternative explanations for low η in the O VI absorbers. Therefore, in the following we present the results of models of a hot gas embedded in the meta-galactic UV background.

We use the photoionization code CLOUDY (v07.02; Ferland et al. 1998) to derive the ionization structure in a gas with fixed temperature (therefore *not* controlled by photoionization). This will make it possible to discuss at the same time both extreme situations (collisional ionization and photoionization) and the intermediate situation of a high-temperature gas with a contribution from photoionization. For comparison, we also show results from the model in which the temperature is the consequence of thermal equilibrium under photoionization. The calculations are made in the optically thin case. We use the MH05 background spectrum dominated

by QSOs as in CLOUDY. We assume relative solar abundances and [C/H] $= -1.0$. In Fig. 9(a), we plot the variation of the O VI to C IV ratio with hydrogen density. The solid black line is the result of model calculations in which temperature is calculated by CLOUDY assuming photoionization equilibrium. Other lines are for temperatures in the range $5 \times 10^4 - 5 \times 10^5$ K. It is to be remembered that, when pure collisional excitation is considered, the fraction of He II is maximum when $4.5 \leq \log T(\text{K}) \leq 4.9$, and in the case of O VI it is when $T \sim 3 \times 10^5$ K (Gnat & Sternberg 2007).

At low temperatures (say $T \leq 5 \times 10^4$ K), the ionization is dominated by photoionization. As expected, the transition between photoionization-dominated and collisional ionization-dominated regimes happens at $T \sim 10^5$ K.

The horizontal dotted lines show the range of observed O VI to C IV column density ratios (between 10 and 20) seen in the C IV components of the two systems discussed above. This range is well reproduced by models with $T \leq 10^5$ K for a typical density of 10^{-4} cm^{-3}. However, the higher O VI to C IV ratio inferred in the velocity range (or Voigt-profile components) in which only O VI is detected needs either a low-density (and low-temperature) photoionized gas or a high-density (i.e $\geq 10^{-3}$ cm^{-3}) hot gas ($T > 10^5$ K), where collisions begin to play a role. Interestingly, such high temperatures are not ruled out by the b-parameters of O VI components (see discussions in the previous section).

In Fig. 9(b) we plot η as predicted by the models versus the hydrogen density. It is apparent that low η values (i.e ≤ 60) are only possible for $T > 10^5$ K. Available data on H I and He II profiles allow for the existence of such a hot gas that would also produce the component with high O VI to C IV column density ratio (i.e $N(\text{O VI})/N(\text{C IV}) \geq 20$). It is apparent from Fig. 4 that the absorption profiles indicate higher Doppler parameters going from C IV to O VI to H I. This has already been noted for C IV and O VI by Fox et al. (2007) and interpreted as the existence of a hot phase. We note that the b values measured for the strongest H I components in the two systems (38.6 km s^{-1} at $z_{abs} = 2.6498$ and 46.6 and 69.5 km s^{-1} at $z_{abs} = 2.6346$; see Tables 1 and 2) are consistent with a temperature
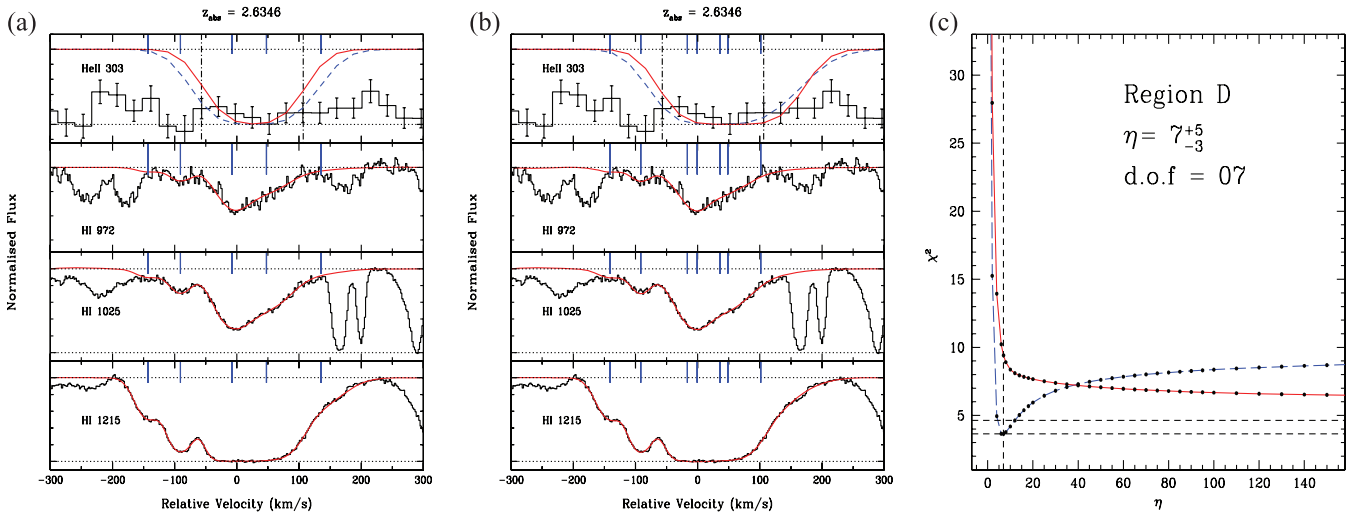
Figure 7. Fits of H I and He II absorption in the $z_{abs} = 2.6346$ system. In all panels, dashed (blue) and solid (red) curves are for turbulent, $\xi = b(\text{He II})/b(\text{H I}) = 1$, and thermal, $\xi = 0.5$, broadening cases, respectively. (a) Fit using the minimum number (five) of components required to fit the H I absorption. The dashed and solid curves in the top panel are the simulated He II profiles with $\eta \sim 12$ and 160, respectively. Only pixels between the two vertical dot–dashed lines are used to derive η by χ^2 minimization. (b) Fit with seven components imposing H I components at the position of the O VI components. The dashed and solid curves in the top panel are the simulated He II profiles with $\eta \sim 7$ and 140, respectively. (c) χ^2 plot for fits shown in (b). Vertical ticks in (a) and (b) indicate the positions of individual Voigt components.
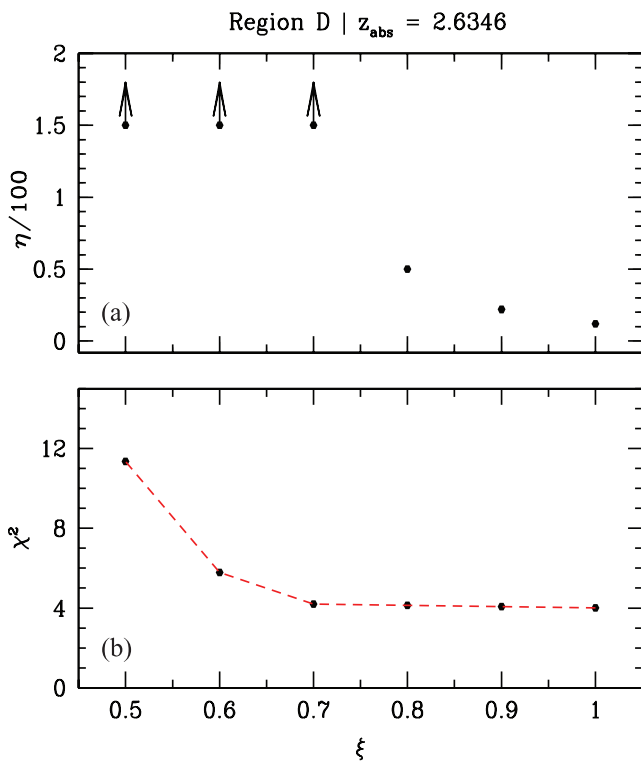

Figure 8. System at $z_{abs} = 2.6346$. (a) Minimum χ^2 as a function of ξ in the case of H I fitted with the minimum number of components. (b) Best-fitting value of η for various values of ξ.

$T \geq 10^5$ K, and it is apparent from the absorption profiles that larger b values could be accommodated.

If the low η values were to be confirmed, we would favour a scenario in which the absorbing gas is a multiphase medium in which photoionized gas components coexist with a wide range of densities and temperatures. While most of the metal absorption

traced by C IV comes from the relatively cold (i.e $T \leq 10^5$ K) gas, part of O VI and predominant contributions of H I and He II could result from a hot phase ($T > 10^5$ K). There is evidence for the existence of multiphase media in the low-redshift O VI absorbers (Tripp et al. 2008) and for O VI absorption associated with high-redshift DLAs (Fox et al. 2007).

6 CONCLUSIONS

We have reanalysed the line of sight towards the high-redshift ($z_{em} = 2.885$) bright quasar QSO HE 2347−4342 and measured the parameter $\eta = N(\text{He II})/N(\text{H I})$ in the Lyman α forest using Voigt-profile fitting of the H I transitions in the Lyman series. As in previous studies, we find that $\eta > 50$ in most of the Lyman α forest, except in four regions where it is much smaller ($\eta \sim 10$–20).

We detect O VI absorption associated with two of these regions (at $z_{abs} = 2.6346$ and 2.6498). The corresponding wavelength ranges for the two other regions are too blended to reach any firm conclusion on the presence of associated O VI absorption. We observe that the $z_{abs} = 2.6346$ system is a usual system with the metals located at the centre of the H I profile, whereas the $z_{abs} = 2.6498$ system has the metals displaced in the red wing of the H I absorption, but, moreover, with the C IV profile systematically shifted compared with O VI. Doppler parameters of the well-defined C IV components rule out the idea that the associated gas is hot and favour the idea that this gas is photoionized. We show that, if we constrain the fit of the H I and/or He II absorption profiles with the presence of metal components, we can accommodate η values in the range 15–100 in these systems, assuming that broadening is intermediate between pure thermal and pure collisional.

We construct constant-density photoionized models and show that, while simple photoionization models reproduce the observed $N(\text{O VI})/N(\text{C IV})$ ratio for a range of densities, they fail to produce low η values. On the contrary, models with high temperatures (i.e $T \geq 10^5$ K) can produce low values of η.

The Doppler parameters of the strongest H I components are consistent with such temperatures. In addition, the higher b values
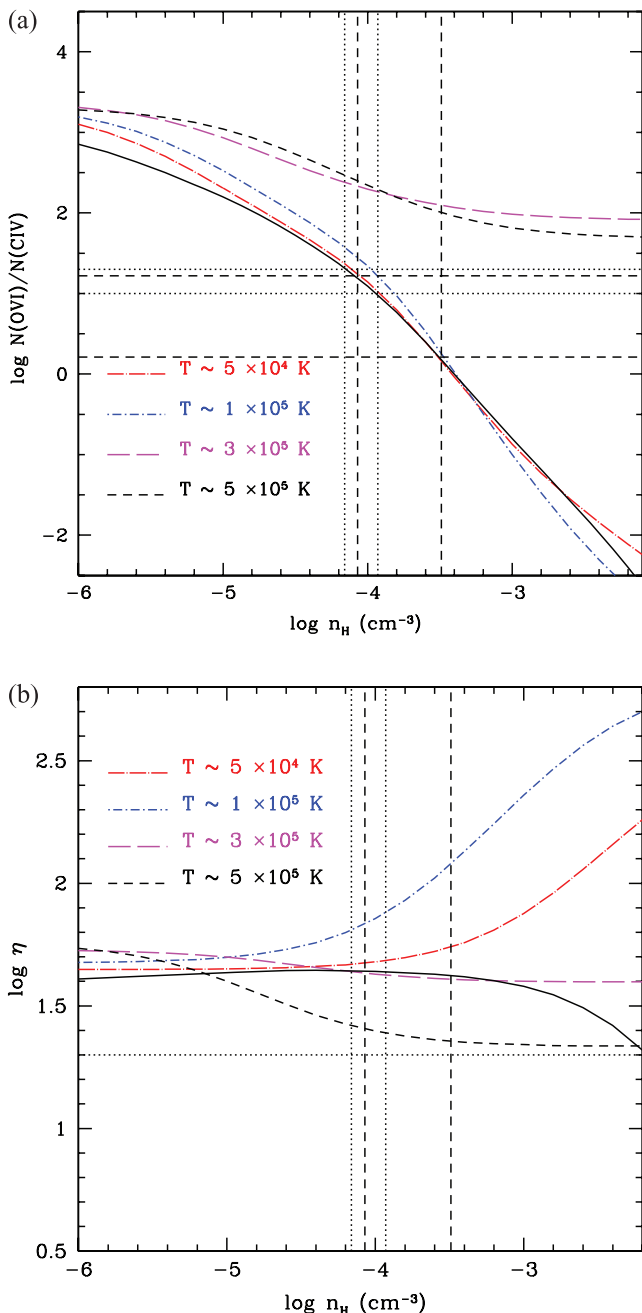
produced by photoionization, we expect the O VI systems with low η to be associated with galaxies. Therefore, it may be interesting to perform a deep search for Lyman-break galaxies at these redshifts in these fields.

ACKNOWLEDGMENTS

REFERENCES

Aguirre A., Dow-Hygelund C., Schaye J., Theuns T., 2008, ApJ, 689, 851
Aracil B., Petitjean P., Pichon C., Bergeron J., 2004, A&A, 419, 811
Ballester P., Modigliani A., Boitquin O., Cristiani S., Hanuschik R., Kauffer A., Wolf S., 2000, The Messenger, 101, 31
Bergeron J., Aracil B., Petitjean P., Pichon C., 2002, A&A, 396, L11
Bergeron J. et al., 2004, The Messenger, 118, 40
Bouché N., Lehnert M. D., Péroux C., 2006, MNRAS, 367, L16
Bouché N., Lehnert M. D., Aguirre A., Péroux C., Bergeron J., 2007, MNRAS, 378, 525
Chand H., Srianand R., Petitjean P., Aracil B., 2004, A&A, 417, 853
Davé R. et al., 2001, ApJ, 552, 473
Dekker H., D'Odorico S., Kaufer A., Delabre B., Kotzlowski H., 2000, in Iye M., Moorwood A. F., eds, Proc. SPIE Vol. 4008, Optical and IR Telescope Instrumentation and Detectors. SPIE, Bellingham, p. 534
Edlén B., 1966, Metrologia, 2, 71
Ellison S. L., Songaila A., Schaye J., Pettini M., 2000, AJ, 120, 1175
Fang T., Bryan G. L., 2001, ApJ, 561, L31
Fardal M. A., Giroux M. L., Shull J. M., 1998, AJ, 115, 2206
Fechner C., Reimers D., 2007, A&A, 461, 847
Ferland G. J., Korista K. T., Verner D. A., Ferguson J. W., Kingdon J. B., Verner E. M., 1998, PASP, 110, 761
Fox A. J., Petitjean P., Ledoux C., Srianand R., 2007, A&A, 465, 171
Gnat O., Sternberg A., 2007, ApJS, 168, 213
Haardt F., Madau P., 1996, ApJ, 461, 20
Kang H., Ryu D., Cen R., Song D., 2005, ApJ, 620, 21
Khare P., Srianand R., York D. G., Green R., Welty D., Huang K., Bechtold J., 1997, MNRAS, 285, 167
Kriss G. A. et al., 2001, Sci, 293, 1112
Oppenheimer B. D., Davé R., 2009, MNRAS, 395, 1875
Pieri M. M., Frank S., Mathur S., Weinberg D. H., York D. G., Oppenheimer B. D., 2010, ApJ, 716, 1084
Reimers D., Kohler S., Wisotzki L., Groote D., Rodriguez-Pascual P., Wamsteker W., 1997, A&A, 327, 890
Scannapieco E., Pichon C., Aracil B., Petitjean P., Thacker R. J., Pogosyan D., Bergeron J., Couchman H. M. P., 2006, MNRAS, 365, 615
Schaye J., Aguirre A., Kim T.-S., Theuns T., Rauch M., Sargent W. L. W., 2003, ApJ, 596, 768
Shull J. M., Tumlinson J., Giroux M. L., Kriss G. A., Reimers D., 2004, ApJ, 600, 570
Shull J. M., France K., Danforth C., Smith B., Tumlinson J., 2010, arXiv:1008.2957
Simcoe R. A., Sargent W. L. W., Rauch M., 2004, ApJ, 606, 92
Smette A., Heap S. R., Williger G. M., Tripp T. M., Jenkins E. B., Songaila A., 2002, ApJ, 564, 542
Songaila A., Cowie L. L., 1996, AJ, 112, 335
Srianand R., Petitjean P., 2000, A&A, 357, 414
Stumpff P., 1980, A&AS, 41, 1
Tripp T. M., Sembach K. R., Bowen D. V., Savage B. D., Jenkins E. B., Lehner N., Richter P., 2008, ApJS, 177, 39
Worseck G., Fechner C., Wisotzki L., Dall'Aglio A., 2007, A&A, 473, 805
Zheng W. et al., 2004, ApJ, 605, 631

This paper has been typeset from a T\[E\]X/L\[A\]T\[E\]X file prepared by the author.

Figure 9. (a) The O VI to C IV column density ratio versus hydrogen density. The different curves correspond to the results of optically thin CLOUDY models with constant temperature, except for the solid black curve, which is for thermal equilibrium. The gas is assumed to have metallicity [C/H] = −1.0 and solar relative abundances and to be exposed to a QSO-dominated ionizing flux. The horizontal dotted and dashed lines show the range of observed column density ratios for the system at z_{abs} = 2.6498 and 2.6346, respectively. The vertical dotted and dashed lines indicate the corresponding allowed range in hydrogen density for photoionization equilibrium.

observed for O VI compared with C IV and the existence of O VI components alone suggest a multiphase nature of the absorbing region. Therefore, if low η values were to be confirmed, we would favour a multiphase model in which most of the gas in the regions of low η is at a high temperature ($>10^5$ K), but the metals, and in particular C IV, are located in lower-temperature photoionized and probably transient regions. As the high-temperature gas cannot be